Inorganic Chemistry

Article

pubs.acs.org/IC

Donor–Acceptor Ligand-to-Ligand Charge-Transfer Coordination Complexes of Nickel(II)

Wesley W. Kramer, Lindsay A. Cameron, Ryan A. Zarkesh, Joseph W. Ziller, and Alan F. Heyduk*

Department of Chemistry, University of California, Irvine, California 92697, United States

Supporting Information

ABSTRACT: A family of charge-transfer chromophores comprising square-planar nickel(II) complexes with one catecholate donor ligand and one α-diimine acceptor ligand is reported. The nine new chromophores were prepared using three different catecholate ligands and three different α-diimine ligands. Single-crystal X-ray diffraction studies on all members of the series confirm a catecholate donor–nickel(II)–α-diimine acceptor electronic structure. The coplanar arrangement of donor and acceptor ligands manifests an intense ligand-to-ligand charge-transfer (LL′CT) absorption band that can be tuned incrementally from 650 nm (1.9 eV) to 1370 nm (0.9 eV). Electrochemical studies of all nine complexes reveal rich redox chemistry with two one-electron reduction processes and two one-electron oxidation processes. For one dye, both the singly reduced anion and the singly oxidized cation were prepared, isolated, and characterized by EPR spectroscopy to confirm ligand-localization of the redox processes. The optical and electrochemical properties of these new complexes identify them as attractive candidates for charge-transfer photochemistry and solar-energy conversion applications.

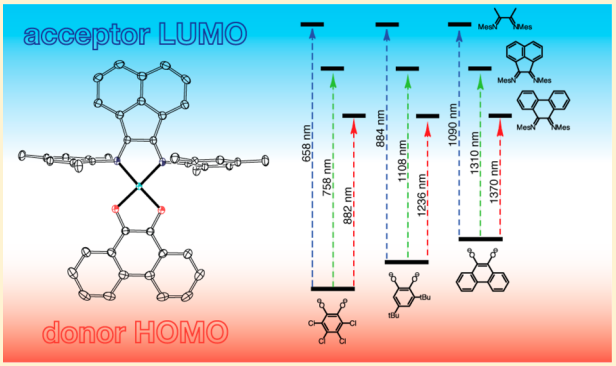

INTRODUCTION

Photoinduced charge separation is the first step in the conversion of light energy to chemical energy. In solid-state devices, photoinduced charge separation occurs by the dissociation of a photogenerated exciton. In molecular systems, the analogous generation of a charge-separated state occurs with supramolecular triads comprising a porphyrin light absorber sandwiched between organic electron donor (D) and electron acceptor (A) moieties.[1−4] Photon absorption by the porphyrin gives an excited state that relaxes to a D^+–porphyrin–A^- charge-separated state by thermal electron transfer. Molecular-level charge separation can also be achieved by direct photoinduced charge-transfer, provided that the dye itself contains localized molecular orbitals to serve as the intramolecular electron donor and acceptor sites.[5,6] The charge-transfer coordination complex, $[Ru^{II}(bpy)_3]^{2+}$, is a classic example of the latter type of dye, in which filled ruthenium(II) orbitals serve as the donor orbitals, while bpy π^* orbitals serve as the acceptor orbitals. The complex exhibits a strong absorption in the visible region of the electromagnetic spectrum corresponding to a charge-transfer that moves an electron from metal to ligand (MLCT) to form an excited state described as $[Ru^{III}(bpy^{\bullet-})(bpy)_2]^{2+}$.[7,8] In principle, it should be possible to design donor–acceptor coordination complexes that combine features of both molecular strategies: specifically, a direct, optical charge-transfer that occurs between distinct organic donors and acceptor ligands (LL′CT). In this way, it may be possible to extensively tune the energetics of the donor–acceptor complex while avoiding the inefficiencies of separate light-absorption and electron-transfer steps.

Quinone-type ligands have well-established redox properties when coordinated to metal ions. As summarized in Chart 1,

Chart 1

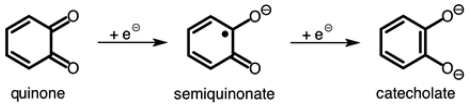

one-electron reduction of *ortho*-quinone affords an *ortho*-semiquinonate. Addition of a second electron affords the fully reduced catecholate. Analogous ligand oxidation states have been established for the related *ortho*-iminoquinone and *ortho*-diiminoquinone (i.e., *ortho*-phenylenediimine) derivatives. Detailed electrochemical studies of $[Ru^{II}(q)(bpy)_2]^{2+}$ derivatives (q = *ortho*-quinone, *ortho*-iminoquinone, or *ortho*-diiminoquinone) established the relative thermodynamic potentials of these three redox-active ligands, showing that for every oxygen atom that is replaced by a nitrogen group (NH), the ligand reduction potential is approximately 0.5 V more negative.[9] In addition, these electrochemical data hint at the implications associated with incorporating two or more redox-active ligands into a single coordination complex. In complexes where the two

Received: July 22, 2014
Published: August 6, 2014

   dx.doi.org/10.1021/ic5017214 | *Inorg. Chem.* 2014, 53, 8825–8837

redox-active ligands are the same, symmetric electron configurations are favored. Indeed, bis(amidophenolate) complexes of nickel, palladium, and platinum along with a plethora of related complexes attest to the favorability of a symmetric $M(sq)_2$ electron configuration (sq = semiquinonate).[10−15] In contrast, for ligands with significantly different redox potentials, the electrochemical data suggest that the favored electron configuration will be asymmetric: one ligand will adopt the reduced catecholate oxidation state, while the other is in the oxidized *ortho*-quinone form. Distinct catecholate and *ortho*-quinone ligands within the coordination sphere of a square-planar metal ion could then serve as donor and acceptor moieties, respectively, for photoinduced charge separation.

Group 10 complexes of redox-active ligands are well established in the literature. Symmetric nickel bis(dithiolene) complexes established the concept of ligand noninnocence, and analogous complexes typically have strong absorption profiles in the visible and NIR portions of the electromagnetic spectrum.[16−18] Nickel dithiolene complexes have received considerable attention for applications in nonlinear optics where it has been shown that less electronically symmetric complexes lead to enhanced nonlinear optical properties.[19,20] The electronic structure and photochemistry of platinum(II) complexes containing a dithiolate donor ligand and a diimine acceptor ligand also have received considerable attention.[21−24] In these complexes, significant orbital mixing between the platinum d orbitals and the dithiolate π^* orbitals leads to a lowest-energy electronic transition that was described as MLL′CT (mixed-metal−ligand-to-ligand charge-transfer). Similarly, platinum(II) complexes containing a catecholate-type donor ligand and a bipyridal acceptor ligand have been elaborated.[25−27] These species show LL′CT absorptions in the visible region of the absorption spectrum (∼600 nm) leading to charge-separated excited states with lifetimes of less than 1 ns.

This Article reports the synthesis and characterization of a new family of donor−acceptor LL′CT chromophores of square-planar nickel(II) centers with the general formulation (catecholate)Ni(diimine). Three different catecholate ligands have been employed as donors (3,5-di-*tert*-butylcatecholate, cat-tBu$_2^{2-}$; tetrachlorocatecholate, catCl_4^{2-}; and 9,10-phenanthrenediolate, pdiol^{2-}), and three different α-diimine ligands have been employed as acceptors (*N*,*N*′-bis(2,4,6-trimethylphenyl)-2,3-butanediimine, bdi; *N*,*N*′-bis(2,4,6-trimethylphenyl)-acenaphthenediimine, adi; and *N*,*N*′-bis(2,4,6-trimethylphenyl)-9,10-phenanthrenediimine, pdi). For these nine new complexes, structural and spectroscopic data confirm that they fit the donor−metal−acceptor model with a reduced catecholate donor ligand and an oxidized α-diimine (diiminoquinone-like) acceptor ligand. The lowest-energy electronic transition is consistent with an LL′CT transition, and the maximum of this absorption shifts from the visible to the near-IR portion of the electromagnetic spectrum depending on the specific combination of catecholate and diimine ligand. Consistent with the LL′CT assignment, the lowest-energy absorption shows a strong sensitivity to the solvent, displaying negative solvatochromism consistent with a polar, donor−acceptor ground state. Cyclic voltammetry studies show that each complex exhibits two reversible one-electron reductions and two partially reversible one-electron oxidations. In one case, bulk chemical oxidation and reduction reactions were used to prepare samples of the dye cation and anion, respectively, and EPR spectroscopy was used to verify that the loci of the redox processes were the redox-active ligands rather than the nickel(II) center. Taken together, the results reported here establish a new family of highly tunable charge-transfer dyes based on an earth abundant metal ion and readily available redox-active ligands. Such complexes should find widespread application in photoinduced electron transfer and solar-energy conversion strategies.

EXPERIMENTAL SECTION

General Considerations. All compounds and reactions reported below show various levels of air- and moisture-sensitivity, so all manipulations were carried out using standard vacuum-line, Schlenk-line, and glovebox techniques. Solvents were sparged with argon before being deoxygenated and dried by passage through Q5 and activated alumina columns, respectively. To test for effective oxygen and water removal, aliquots of each solvent were treated with a few drops of a purple solution of sodium benzophenone ketyl radical in THF. The reagents 3,5-di-*tert*-butyl-1,2-quinone (Aldrich), tetrachloro-1,2-quinone (Acros), phenanthrenequinone (Acros), and Ni(cod)$_2$ (Strem) were reagent grade or better and used as received. The diimine ligands *N*,*N*′-bis(2,4,6-trimethylphenyl)-2,3-butanediimine (bdi),[28] *N*,*N*′-bis(2,4,6-trimethylphenyl)acenaphthenediimine (adi),[29] and *N*,*N*′-bis(2,4,6-trimethylphenyl)-9,10-phenanthrenediimine (pdi)[30] were prepared according to published procedures.

Spectroscopic Measurements. NMR spectra were collected at 298 K on a Bruker Avance 500 MHz spectrometer in dry, degassed $CDCl_3$, d_8-THF, or C_6D_6. ^{1}H NMR spectra were referenced to tetramethylsilane (TMS) using the residual proteo impurities of the solvent (7.26 ppm for $CDCl_3$, 3.58 ppm for d_8-THF, 7.16 ppm for C_6D_6); ^{13}C NMR spectra were referenced to TMS using the natural ^{13}C abundance of the solvent (77.16 ppm for $CDCl_3$, 25.37 ppm for d_8-THF, 128.06 ppm for C_6D_6). All chemical shifts are reported using the standard δ notation in parts per million; positive chemical shifts are to a higher frequency from the given reference. Electronic absorption spectra were recorded with a PerkinElmer Lambda 900 UV−vis−NIR spectrophotometer using 1 cm path-length cells at ambient temperature (20−24 °C). Perpendicular-mode X-band EPR spectra were collected using a Bruker EMX spectrometer equipped with an ER041XG microwave bridge using the following spectrometer settings: attenuation = 20 dB, microwave power = 2.017 mW, frequency = 9.79 GHz,, modulation amplitude = 1.02 G, gain = 2.00 × 10^3, conversion time = 81.92 ms, time constant = 655.36 ms, sweep width = 300 G, and resolution = 1024 points. The EPR spectra were modeled using EasySpin.[31]

Electrochemical Methods. Electrochemical experiments were performed on a Gamry Series G300 potentiostat/galvanostat/ZRA (Gamry Instruments, Warminster, PA) using a 3.0 mm glassy carbon working electrode, a platinum wire auxiliary electrode, and a silver wire reference electrode. Reversibility was judged on the basis of the ratio of the anodic (i_{pa}) to the cathodic (i_{pc}) current being close to unity for a given process. Electrochemical experiments were performed at ambient temperature (20−24 °C) in a nitrogen-filled glovebox on either THF or CH_2Cl_2 solutions. Sample concentrations were 1.0 mM in analyte and with 100 mM $[NBu_4][PF_6]$ as the supporting electrolyte. All potentials are referenced to $[Cp_2Fe]^{+/0}$ using ferrocene or decamethylferrocene (−0.49 V vs $[Cp_2Fe]^{+/0}$)[32] as an internal standard added at the end of a sample run. Ferrocene and decamethylferrocene (Acros) were purified by sublimation under reduced pressure, and tetrabutylammonium hexafluorophosphate (Acros) was recrystallized from ethanol three times and dried under a vacuum.

X-ray Data Collection and Refinement. X-ray diffraction data for all complexes were collected on single crystals mounted on a glass fiber using Paratone oil. Data were acquired using a Bruker CCD platform diffractometer equipped with a CCD detector at 143 K using Mo Kα (λ = 0.71073 Å) radiation, which was wavelength selected with a single-crystal graphite monochromator. The SMART program

dx.doi.org/10.1021/ic5017214 | Inorg. Chem. 2014, 53, 8825−8837

package was used to determine unit-cell parameters and for data collection. The raw frame data were processed using SAINT and SADABS to yield the reflection data file. Subsequent calculations were carried out using the SHELXTL program suite.[33] Analytical scattering factors for neutral atoms were used throughout the analyses.[34] Hydrogen atoms were generated in calculated positions and refined using a riding model. ORTEP diagrams were generated using *ORTEP-3* for Windows.[35] Unit cell and diffraction data for all complexes are given in the Supporting Information.

General (Catecholate)Ni(diimine) Synthesis, Method A. A solution of $Ni(cod)_2$ in 10 mL of benzene or toluene was treated with the appropriate diimine ligand as a solid. The solution was stirred at ambient temperature for 12 h during which time the solution color changed from yellow to red or purple. Solid quinone was then added to the solution, resulting in the formation of a dark suspension/solution over the course of 3 h. For complexes incorporating the tetrachlorocatecholate ligand, the reaction mixture was filtered through a sintered glass frit to obtain the product as a darkly colored solid. In the case of complexes incorporating the 3,5-di-*tert*-butylcatecholate and 9,10-phenanthrenediolate ligands, the solution volume was reduced under vacuum, diluted with pentane, and chilled to −35 °C. The resulting precipitate was collected by filtration, washed with aliquots of cold pentane, and dried under reduced pressure to obtain the desired product as a darkly colored solid.

General (Catecholate)Ni(diimine) Synthesis, Method B. A frozen solution containing 3,5-di-*tert*-butylcatechol in THF was thawed and immediately treated with 2 equiv of *n*BuLi (2.49 M in hexanes). The mixture was stirred and allowed to warm to room temperature before being combined with a suspension of $(dme)NiCl_2$ in 10 mL of THF. The reaction was stirred for 12 h at ambient temperature to afford a red-orange solution, which was treated with a solid portion of the appropriate diimine ligand. The reaction mixture was stirred for an additional 12 h before the solvent was removed under reduced pressure. The solid residue was coevaporated with Et_2O and pentane and then extracted with toluene and filtered to remove LiCl. The volume of the filtrate was reduced, diluted with pentane, and cooled to −35 °C. A first crop of the product was collected from the cold solution by filtration. A second crop of product was obtained by reprocessing the filtrate.

Synthesis of (cat-*t*Bu$_2$)Ni(bdi) (1a). Complex **1a** was prepared according to Method A using *N*,*N*′-bis(2,4,6-trimethylphenyl)-2,3-butanediimine (160 mg, 0.50 mmol, 1.0 equiv), $Ni(cod)_2$ (138 mg, 0.50 mmol, 1.0 equiv), and 3,5-di-*tert*-butyl-*o*-benzoquinone (110 mg, 0.50, 1.0 equiv). The product was isolated as a dark green solid in 77% yield (231 mg).

The preparation of **1a** by Method B proceeded using 222 mg of 3,5-di-*tert*-butylcatechol (1.0 mmol, 1 0.0 equiv), 220 mg of $(dme)NiCl_2$ (1.0 mmol, 1.0 equiv), and 320 mg of *N*,*N*′-bis(2,4,6-trimethylphenyl)-2,3-butanediimine (1.0 mmol, 1.0 equiv). The product was isolated as a dark green solid in 76% yield (454 mg). Layering a solution of **1a** in toluene with pentane afforded X-ray quality crystals.

Anal. Calcd for $C_{36}H_{48}N_2O_2Ni$: C, 72.13; H, 8.07; N, 4.67. Found: C, 71.93; H, 8.13; N, 4.37. ^{1}H NMR ($CDCl_3$, 500 MHz) δ/ppm: 0.90 (s, 9H, *t*Bu), 1.12 (s, 9H, *t*Bu), 1.56 (s, 3H, N=CMe), 1.63 (s, 3H, N=CMe), 2.32 (s, 12H, *o*-Me), 2.36 (s, 6H, *p*-Me), 6.24 (s, 2H, cat-*H*), 6.94 (s, 2H, aryl-*H*), 6.96 (s, 2H, aryl-*H*). ^{13}C NMR ($CDCl_3$, 125.8 MHz) δ/ppm: 167.0 (*C*=N), 166.5 (*C*=N), 161.8 (*C*−O), 157.5 (*C*−O), 142.3 (aryl-*C*), 137.7 (aryl-*C*), 136.5 (aryl-*C*), 136.4 (aryl-*C*), 134.5 (aryl-*C*), 130.2 (aryl-*C*), 129.8 (aryl-*C*), 128.8 (aryl-*C*), 110.6 (aryl-*C*), 110.1 (aryl-*C*), 34.4 ($C(CH_3)_3$), 34.2 ($C(CH_3)_3$), 32.4 ($C(CH_3)_3$), 29.5 ($C(CH_3)_3$), 21.6 (*p*-CH_3), 21.4 (*p*-CH_3), 18.8 (*o*-CH_3), 18.7 (*o*-CH_3), 17.9 (N=C−CH_3). UV−vis−NIR (CH_2Cl_2) λ_{max}/nm (ε/M^{-1} cm^{-1}): 308 (13 700), 816 (6510).

Synthesis of (cat-*t*Bu$_2$)Ni(adi) (1b). Complex **1b** was prepared according to Method A using *N*,*N*′-bis(2,4,6-trimethylphenyl)-acenaphthenediimine (212 mg, 0.50 mmol, 1.0 equiv), $Ni(cod)_2$ (138 mg, 0.50 mmol, 1.0 equiv), and 3,5-di-*tert*-butyl-*o*-benzoquinone (110 mg, 0.50, 1.0 equiv). The product was isolated as a yellow-green solid in 86% yield (299 mg).

The preparation of **1b** by Method B proceeded using 506 mg of 3,5-di-*tert*-butylcatechol (2.28 mmol, 1.0 equiv), 500 mg of $(dme)NiCl_2$ (2.28 mmol, 1.0 equiv), and 946 mg of *N*,*N*′-bis(2,4,6-trimethylphenyl)acenaphthenediimine (2.28 mmol, 1.0 equiv). The product was isolated as a yellow-green solid in 77% yield (122 mg). X-ray quality crystals were grown by vapor diffusion of pentane into a solution of **1b** in toluene.

Anal. Calcd for $C_{44}H_{48}N_2O_2Ni$: C, 75.98; H, 6.96; N, 4.03. Found: C, 75.45; H, 7.30; N, 3.68. ^{1}H NMR ($CDCl_3$, 500 MHz) δ/ppm: 0.98 (s, 9H, *t*Bu), 1.16 (s, 9H, *t*Bu), 2.41 (s, 6H *p*-Me), 2.51 (s, 12H, *o*-Me), 6.30 (s, 1H, cat-H), 6.39 (s, 1H, cat-H), 6.77 (broad s, 2H, aryl-H), 7.05 (s, 4H, aryl-H), 7.39 (t, $^3J_{HH}$ = 7.7 Hz, 2H, aryl-*H*), 7.98 (d, $^3J_{HH}$ = 8.3 Hz, 2H, Ar-*H*). ^{13}C NMR ($CDCl_3$ 125.8 MHz) δ/ppm: 162.1 (*C*=N), 157.9 (*C*−O), 143.3 (aryl-*C*), 142.0 (aryl-*C*), 138.6 (aryl-*C*), 136.9 (aryl-*C*), 135.2 (aryl-*C*), 131.5 (aryl-*C*), 130.1 (aryl-*C*), 129.8 (aryl-*C*), 129.3 (aryl-*C*), 127.0 (aryl-*C*), 122.9 (aryl-*C*), 111.0 (aryl-*C*), 110.8 (aryl-*C*), 34.2 ($C(CH_3)_3$), 34.1 ($C(CH_3)_3$), 32.2 ($C(CH_3)_3$), 29.3 ($C(CH_3)_3$), 21.4 (*p*-CH_3), 18.6 (*o*-CH_3). UV−vis−NIR (CH_2Cl_2) λ_{max}/nm (ε/M^{-1} cm^{-1}): 320 (24 400), 426 (5490), 1026 (10 400).

Synthesis of (cat-*t*Bu$_2$)Ni(pdi) (1c). Complex **1c** was prepared according to Method A using *N*,*N*′-bis(2,4,6-trimethylphenyl)-9,10-phenanthrenediimine (221 mg, 0.500 mmol, 1.0 equiv), $Ni(cod)_2$ (138 mg, 0.500 mmol, 1.0 equiv), and 3,5-di-*tert*-butyl-*o*-benzoquinone (110 mg, 0.500 mmol, 1.0 equiv). The product was isolated as a dark red solid in 86% yield (298 mg).

The preparation of **1c** by Method B proceeded using 222 mg of 3,5-di-*tert*-butylcatechol (1.00 mmol, 1.0 equiv), 220 mg of $(dme)NiCl_2$ (1.00 mmol, 1.0 equiv), and 443 mg of *N*,*N*′-bis(2,4,6-trimethylphenyl)-9,10-phenanthrenediimine (1.00 mmol, 1 equiv). The product was isolated as a dark red solid in 77% yield (556 mg). X-ray quality crystals were grown by vapor diffusion of pentane into a solution of **1c** in toluene.

Anal. Calcd for $C_{46}H_{50}N_2O_2Ni$: C, 76.57; H, 6.98; N, 3.88. Found: C, 76.41; H, 7.33; N, 3.75. ^{1}H NMR ($CDCl_3$, 500 MHz) δ/ppm: 0.99 (s, 9H, *t*Bu), 1.16 (s, 9H, *t*Bu), 2.33 (s, 12H, *o*-Me), 2.45 (s, 6H, *p*-Me), 6.37 (s, 1H, cat-*H*), 6.38 (s, 1H, cat-*H*), 7.03−7.06 (m, 5H, aryl-*H*), 7.36 (d, $^3J_{HH}$ = 8.5 Hz, 2H, aryl-*H*), 7.61 (t, $^3J_{HH}$ = 7.5 Hz, 2H, aryl-*H*), 8.16 (d, $^3J_{HH}$ = 7.7 Hz, 2H, aryl-*H*). ^{13}C NMR ($CDCl_3$, 125.8 MHz) δ/ppm: 163.4 (*C*−O), 160.0 (*C*−O), 156.6 (*C*=N), 146.3 (aryl-*C*), 141.1 (aryl-*C*), 137.0 (aryl-*C*), 136.6 (aryl-*C*), 132.0 (aryl-*C*), 130.6 (aryl-*C*), 130.3 (aryl-*C*), 129.4 (aryl-*C*), 129.0 (aryl-*C*), 127.5 (aryl-*C*), 126.8 (aryl-*C*), 124.6 (aryl-*C*), 113.0 (aryl-*C*), 111.9 (aryl-*C*), 34.3 ($C(CH_3)_3$), 34.2 ($C(CH_3)_3$), 32.0 ($C(CH_3)_3$), 29.4 ($C(CH_3)_3$), 21.6 (*p*-CH_3), 19.0 (*o*-CH_3). UV−vis−NIR (CH_2Cl_2) λ_{max}/nm (ε/M^{-1} cm^{-1}): 260 (35 400), 512 (2840), 1186 (16 500).

Synthesis of (catCl$_4$)Ni(bdi) (2a). Complex **2a** was prepared according to Method A using *N*,*N*′-bis(2,4,6-trimethylphenyl)-2,3-butanediimine (117 mg, 0.364 mmol, 1.0 equiv), $Ni(cod)_2$ (100 mg, 0.364 mmol, 1.0 equiv), and tetrachloro-1,2-quinone (89 mg, 0.364 mmol, 1.0 equiv). The product was isolated as a dark blue solid in 88% yield (199 mg). X-ray quality crystals were grown by slow evaporation of a CH_2Cl_2 solution of **2a**.

Anal. Calcd for $C_{28}H_{28}N_2O_2Cl_4Ni$: C, 53.80; H, 4.42; N, 4.48. Found: C, 53.93; H, 4.37; N, 4.07. ^{1}H NMR ($CDCl_3$, 500 MHz) δ/ppm: 1.84 (s, 6H, N=CMe), 2.44 (s, 12H, *o*-Me), 2.34 (s, 6H, *p*-Me), 7.00 (s, 4H, aryl-*H*). ^{13}C NMR ($CDCl_3$, 125.8 MHz) δ/ppm: 171.0 (*C*=N), 157.6 (*C*−O), 140.5 (aryl-*C*), 137.9 (aryl-*C*), 130.1 (aryl-*C*), 129.3 (aryl-*C*), 117.1 (aryl-*C*), 115.5 (aryl-*C*), 21.5 (*p*-CH_3), 18.9 (*o*-CH_3), 18.4 (CH_3). UV−vis−NIR (CH_2Cl_2) λ_{max}/nm (ε/M^{-1} cm^{-1}): 320 (12 400), 670 (5280).

Synthesis of (catCl$_4$)Ni(adi) (2b). Complex **2b** was prepared according to Method A using *N*,*N*′-bis(2,4,6-trimethylphenyl)-acenaphthenediimine (152 mg, 0.364 mmol, 1.0 equiv), $Ni(cod)_2$ (100 mg, 0.364 mmol, 1.0 equiv), and tetrachloro-1,2-quinone (89 mg, 0.364 mmol, 1.0 equiv). The product was isolated as a dark green solid in 86% yield (225 mg). X-ray quality crystals were grown by vapor diffusion of pentane into a THF solution of the product.

Anal. Calcd for $C_{36}H_{28}N_2O_2Cl_4Ni$: C, 59.96; H, 3.91; N, 3.88. Found: C, 59.86; H, 3.91; N, 3.77. ^{1}H NMR ($CDCl_3$, 500 MHz) δ/

dx.doi.org/10.1021/ic5017214 | *Inorg. Chem.* 2014, 53, 8825−8837

ppm: 2.41 (s, 6H, *p*-Me), 2.56 (s, 12H, *o*-Me), 6.87 (d, $^3J_{HH}$ = 7.0 Hz, 2H, aryl-*H*), 7.07 (s, 4H, aryl-*H*), 7.50 (t, $^3J_{HH}$ = 7.7 Hz, 2H, aryl-*H*), 8.08 (d, $^3J_{HH}$ = 8.4 Hz, 2H, aryl-*H*). ^{13}C NMR ($CDCl_3$, 125.8 MHz) δ/ppm: 169.2 (*C*═N), 157.5 (*C*−O), 146.0 (aryl-*C*), 140.1 (aryl-*C*), 138.0 (aryl-*C*), 131.9 (aryl-*C*), 131.4 (aryl-*C*), 130.4 (aryl-*C*), 129.5 (aryl-*C*), 129.5 (aryl-*C*), 125.5 (aryl-*C*), 124.3 (aryl-*C*), 117.1 (aryl-*C*), 21.5 (aryl-CH_3), 18.8 (aryl-CH_3). UV−vis−NIR (CH_2Cl_2) λ_{max}/nm (ε/M^{-1} cm^{-1}): 328 (23 700), 748 (7260).

Synthesis of (catCl$_4$)Ni(pdi) (2c). Complex **2c** was prepared according to Method A using *N*,*N*′-bis(2,4,6-trimethylphenyl)-9,10-phenanthrenediimine (161 mg, 0.36 mmol, 1.0 equiv), Ni(cod)$_2$ (100 mg, 0.36 mmol, 1.0 equiv), and tetrachloro-1,2-quinone (89 mg, 0.36 mmol, 1.0 equiv). The product was isolated as a dark red-orange solid in 88% yield (238 mg). X-ray quality crystals were grown from a CH_2Cl_2 solution of the **2c** chilled to −35 °C.

^{1}H NMR ($CDCl_3$, 500 MHz) δ/ppm: 2.38 (s, 12H, *o*-Me), 2.40 (s, 6H, *p*-Me), 7.08 (s, 4H, aryl-*H*), 7.12 (t, $^3J_{HH}$ = 7.8 Hz, 2H, aryl-*H*), 7.48 (d, $^3J_{HH}$ = 8.4 Hz, 2H, aryl-*H*), 7.68 (t, $^3J_{HH}$ = 7.5 Hz, 2H, aryl-*H*), 8.12 (d, $^3J_{HH}$ = 8.1 Hz, 2H, aryl-*H*). ^{13}C NMR ($CDCl_3$, 125.8 MHz) δ/ppm: 160.1 (*C*═N), 157.2 (*C*−O), 144.4 (aryl-*C*), 137.9 (aryl-*C*), 133.5 (aryl-*C*), 133.1 (aryl-*C*), 130.0 (aryl-*C*), 129.8 (aryl-*C*), 128.3 (aryl-*C*), 126.5 (aryl-*C*), 125.0 (aryl-*C*), 117.8 (aryl-*C*), 115.9 (aryl-*C*), 21.5 (*p*-CH_3), 19.1 (*o*-CH_3). UV−vis−NIR (CH_2Cl_2) λ_{max}/nm (ε/M^{-1} cm^{-1}): 352 (12 600), 876 (10 000).

Synthesis of (pdiol)Ni(bdi) (3a). Complex **3a** was prepared according to Method A using *N*,*N*′-bis(2,4,6-trimethylphenyl)-2,3-butanediimine (160 mg, 0.5 mmol, 1 equiv), Ni(cod)$_2$ (138 mg, 0.50 mmol, 1 equiv), and 9,10-phenanthrenequinone (104 mg, 0.50 mmol, 1 equiv) in benzene. The product was isolated as a green microcrystalline solid and purified by recrystallization with THF and pentane and subsequent washing with cold pentane to yield a forest green microcrystalline solid (189 mg, 64% yield). X-ray quality crystals were grown by vapor diffusion of pentane into a solution of **3a** in THF.

Anal. Calcd for $C_{36}H_{36}N_2O_2Ni$: C, 73.61; H, 6.18; N, 4.77. Found: C, 73.23; H, 6.13; N, 4.46. ^{1}H NMR (500 MHz; d_8-THF) δ/ppm: 1.74 (s, 6H, N═CMe), 1.74 (s, 6H, N═CMe), 2.40 (s, 6H, *p*-Me), 2.48 (s, 12H, *o*-Me), 7.05 (m, 8H), 7.36 (d, $^3J_{HH}$ = 7.8, 2H, aryl-*H*), 8.27 (d, $^3J_{HH}$ = 7.9, 2H, aryl-*H*). ^{13}C NMR (126 MHz; d_8-THF) δ/ppm: 169.2 (*C*═N), 151.6 (*C*−O), 143.0 (aryl-*C*), 137.0 (aryl-*C*), 131.7 (aryl-*C*), 129.5 (aryl-*C*), 129.3 (aryl-*C*), 129.1 (aryl-*C*), 125.5 (aryl-*C*), 125.0 (aryl-*C*), 122.6 (aryl-*C*), 121.4 (aryl-*C*), 120.6 (aryl-*C*), 21.6 (*p*-CH_3), 19.1 (*o*-CH_3), 17.8 (N═C−CH_3). UV−vis−NIR [THF; λ_{max}/nm (ε/M^{-1} cm^{-1})]: 420 (3500), 1090 (8500).

Synthesis of (pdiol)Ni(adi) (3b). Complex **3b** was prepared according to Method A using *N*,*N*′-bis(2,4,6-trimethylphenyl)-acenaphthenediimine (104 mg, 0.25 mmol, 1 equiv), Ni(cod)$_2$ (69 mg, 0.25 mmol, 1 equiv), and 9,10-phenanthrenequinone (52 mg, 0.25 mmol, 1 equiv) in benzene. The product was isolated as a brownish green solid. X-ray quality crystals of **3b** were obtained by layering a THF solution of the complex with pentane (70 mg, 47% yield).

^{1}H NMR (500 MHz; d_8-THF) δ/ppm: 2.47 (s, 6H, *p*-Me), 2.61 (s, 12H, *o*-Me), 6.81 (s, 2H, aryl-*H*), 7.16 (m, 8H, aryl-*H*), 7.29 (s, 1H, aryl-*H*), 7.45 (s, 2H, aryl-*H*), 7.51 (s, 2H, aryl-H), 8.32 (s, 2H, aryl-H). ^{13}C NMR (126 MHz; d_8-THF) δ/ppm: 166.3 (*C*═N), 152.2 (*C*−O), 142.6 (aryl-*C*), 142.1 (aryl-*C*), 136.7 (aryl-*C*), 131.6 (aryl-*C*), 131.4 (aryl-*C*), 129.9 (aryl-*C*), 129.3 (aryl-*C*), 128.8 (aryl-*C*), 128.1 (aryl-*C*), 127.3 (aryl-*C*), 125.5 (aryl-*C*), 124.6 (aryl-*C*), 122.3 (aryl-*C*), 121.9 (aryl-*C*), 121.7 (aryl-*C*), 120.0 (aryl-*C*), 20.5 (*p*-CH_3), 17.9 (*o*-CH_3). UV−vis−NIR [THF; λ_{max}/nm (ε/M^{-1} cm^{-1})]: 328 (25 054), 1310 (9920).

Synthesis of (pdiol)Ni(pdi) (3c). Complex **3c** was prepared according to Method A using *N*,*N*′-bis(2,4,6-trimethylphenyl)-9,10-phenanthrenediimine (180 mg, 0.25 mmol, 1 equiv), Ni(cod)$_2$ (69 mg, 0.25 mmol, 1 equiv), and 9,10-phenanthrenequinone (52 mg, 0.25 mmol, 1 equiv) in benzene. Recrystallization with benzene and pentane yielded the product as a dark brown/amber microcrystalline solid (150 mg, 85% yield). Layering a benzene solution of **3c** with pentane resulted in the precipitation of X-ray quality crystals.

Anal. Calcd for $C_{46}H_{38}N_2O_2Ni$: C, 77.87; H, 5.40; N, 3.95. Found: C, 77.55; H, 7.30; N, 3.62. ^{1}H NMR (400 MHz; C_6D_6) δ/ppm: 2.39 (s, 6H, *o*-Me), 2.50 (s, 12H, *p*-Me), 6.83 (t, *J* = 7.8, 2H, aryl-*H*), 7.05 (s, 4H, Mes-*H*), 7.08−7.14 (m, 4H, aryl-*H*), 7.32 (t, $^3J_{HH}$ = 7.5, 2H, aryl-*H*), 7.83 (d, $^3J_{HH}$ = 8.4, 2H, aryl-*H*), 7.79 (d, $^3J_{HH}$ = 8.6, 2H, aryl-*H*), 7.97 (d, $^3J_{HH}$ = 7.8, 2H, aryl-*H*), 8.08 (d, $^3J_{HH}$ = 8.1, 2H, aryl-H). ^{13}C NMR (126 MHz; C_6D_6) δ/ppm: 161.2 (*C*−O), 154.0 (*C*═N), 147.5 (aryl-*C*), 136.2 (aryl-*C*), 133.3 (aryl-*C*), 131.1 (aryl-*C*), 128.9 (aryl-*C*), 128.8 (aryl-*C*), 128.6 (aryl-*C*), 128.4 (aryl-*C*), 128.4 (aryl-*C*), 127.9 (aryl-*C*), 126.6 (aryl-*C*), 126.0 (aryl-*C*), 125.7 (aryl-*C*), 124.6 (aryl-*C*), 123.2 (aryl-*C*), 122.4 (aryl-*C*), 21.6 (*p*-CH_3), 19.6 (*o*-CH_3). UV−vis−NIR [THF; λ_{max}/nm (ε/M^{-1} cm^{-1})]: 370 (1600), 1370 (43 000).

Oxidation of (cat-*t*Bu$_2$)Ni(adi) (1b). Solid AgOTf (108 mg, 0.419 mmol, 1.0 equiv) was added to a stirred solution of **1b** (292 mg, 0.419 mmol, 1.0 equiv) in 10 mL of MeCN. An immediate change in the solution color from green to brown occurred with concomitant precipitation of a dark solid. The reaction mixture was stirred for 12 h and then filtered. The solvent was removed from the filtrate under reduced pressure, and the residue was washed three times with Et_2O. The product, [(cat-*t*Bu$_2$)Ni(adi)][OTf], [**1b**][OTf], was isolated as a brown solid in 96% yield (341 mg). UV−vis−NIR (MeCN) λ_{max}/nm (ε/M^{-1} cm^{-1}): 390 (3250), 786 (655).

Reduction of (cat-*t*Bu$_2$)Ni(adi) (1b). A cold (−35 °C) solution of **1b** (300 mg, 0.431 mmol, 1.0 equiv) in MeCN was combined with decamethylcobaltocene (142 mg, 0.431 mmol, 1.0 equiv) and stirred at ambient temperature for 30 h. The solvent was removed under reduced pressure. The green residue was washed with toluene and then with pentane to afford the product, [Cp*$_2$Co][(cat-*t*Bu$_2$)Ni(adi)], [Cp*$_2$Co][**1b**], in 94% yield (417 mg). UV−vis−NIR (MeCN) λ_{max}/nm (ε/M^{-1} cm^{-1}): 434 (4880), 774 (5050).

RESULTS

Synthesis of Donor−Acceptor Complexes. Donor−acceptor complexes of nickel(II) were prepared readily by taking advantage of the ability of *ortho*-quinones to act as two-electron oxidants. The installation of catecholate and semiquinonate ligands by the redox reaction of *ortho*-quinones with reduced metal complexes is well precedented for the preparation of homoleptic complexes of chromium, molybdenum, and tungsten.[36−40] Following these examples, and according to Scheme 1a, a nickel(0) synthon, Ni(cod)$_2$, was treated initially with *N*,*N*′-bis(2,4,6-trimethylphenyl)-2,3-butanediimine (bdi). Although the putative nickel(0) diimine intermediate was not isolated, similar species have been reported in the literature,[41] and its formation is implicated in this case by the development of a dark burgundy solution upon combination of Ni(cod)$_2$ and the bdi ligand. The subsequent addition of 3,5-di-*tert*-butyl-1,2-quinone resulted in a color change to dark green and afforded the square-planar nickel complex, (cat-*t*Bu$_2$)Ni(bdi) (**1a**), in 77% yield. The same protocol worked for the preparation of other α-diimine-nickel species, giving (cat-*t*Bu$_2$)Ni(adi) (**1b**; adi = *N*,*N*′-bis(2,4,6-trimethylphenyl)acenaphthenediimine) and (cat-*t*Bu$_2$)Ni(pdi) (**1c**; pdi = *N*,*N*′-bis(2,4,6-trimethylphenyl)-9,10-phenanthrenediimine) complexes in good yields (77−88%). Changing the quinone gave analogous results, with tetrachloro-1,2-quinone affording (catCl$_4$)Ni(bdi) (**2a**), (catCl$_4$)Ni(adi) (**2b**), and (catCl$_4$)Ni(pdi) (**2c**) complexes and phenanthrenequinone affording (pdiol)Ni(bdi) (**3a**), (pdiol)Ni(adi) (**3b**), and (pdiol)Ni(pdi) (**3c**) complexes.

To avoid the use of the nickel(0) starting material, an alternative strategy for the preparation of nickel donor−acceptor complexes was developed (Scheme 1b). Deprotonation of 3,5-di-*tert*-butylcatechol with 2 equiv of *n*BuLi followed by addition of (dme)NiCl$_2$ in THF afforded a red-orange

dx.doi.org/10.1021/ic5017214 | Inorg. Chem. 2014, 53, 8825−8837

Scheme 1. Synthetic Procedures and (Catecholate)Ni(diimine) Complexes Discussed in This Article

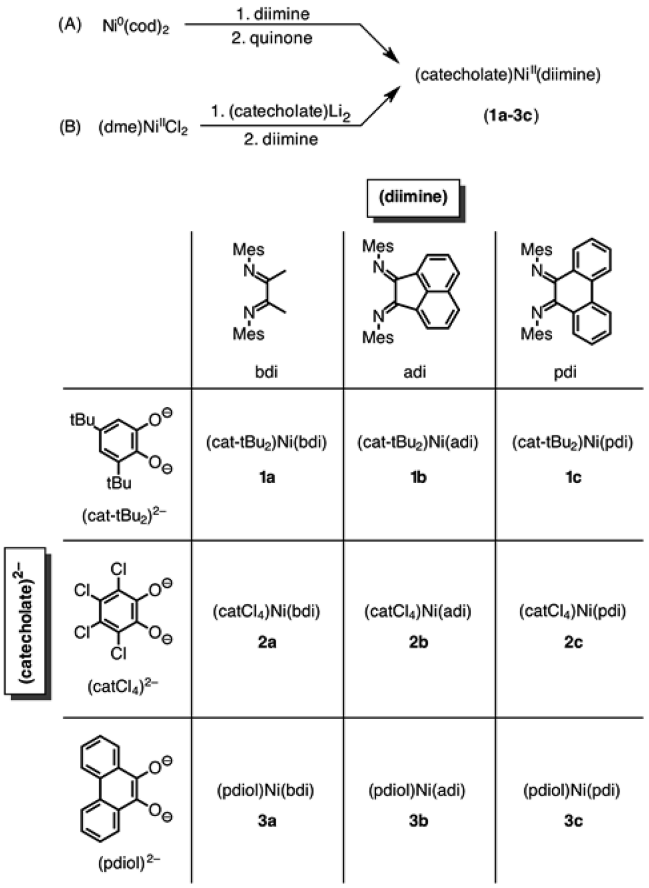

solution of (cat-tBu$_2$)Ni(dme) that was treated in situ with the appropriate α-diimine to afford complexes **1a**−**1c** in good yields (76−77%).

Structural Characterization. Nickel complexes **1**−**3** have two different redox-active ligands, leading to multiple possible experimental oxidation state assignments,[42] so high-resolution, single-crystal X-ray diffraction studies were conducted on all nine members of the series. Figure 1 shows the molecular structures of complexes **1**−**3**, and Table 1 shows pertinent bond distances within the nickel coordination spheres. All complexes have four-coordinate, square-planar nickel centers with no regular distortion pattern within the family of complexes. The largest deviation from planarity within the NiN_2O_2 unit is for (catCl$_4$)Ni(bdi) (**2a**), which is ruffled, displacing the nickel by 0.046 Å from the NiN_2O_2 mean plane. The phenanthrenediimine ligand in the (cat-tBu$_2$)Ni(pdi) complex, **1c**, is distorted to a hyperbolic paraboloid (i.e., saddle shaped), but in the corresponding (catCl$_4$)Ni(pdi) (**2c**) and (pdiol)Ni(pdi) (**3c**) complexes the diimine ligand is planar. The bite angles of the catecholate and diimine ligands are remarkably consistent for complexes **1**−**3** with O−Ni−O bite angles in the range 87.0−89.7° and N−Ni−N bite angles in the range 82.9−85.3°. Complexes **1c** and **3b** are the only structures to show noteworthy packing arrangements in the solid state. In the case of **1c**, the chlorides of the tetrachlorocatecholate ligand are directed into the π system of an adjacent phenanthrene ring,[43] whereas in the case of **3b**, extensive π-stacking interactions exist between neighboring dye molecules.

Bond distances within the nickel complexes are remarkably similar and are consistent with formal oxidation state assignments of nickel(II) metal ions, dianionic catecholates, and neutral α-diimines.[42,44] Catecholate C−O distances of 1.35−1.36 Å in **1a**−**c** and **3a**−**b** are identical to the C−O distances in the bis(catecholate) complex $[Ni(cat)_2]^{2-}$.[45] For complex **3c**, the C−O bond distances are slightly shorter at 1.33 and 1.34 Å, but these distances are still longer than the C−O distances in the bis(semiquinonate) complex Ni(sq-3,6-tBu$_2$)$_2$ (d_{C-O} = 1.31 Å).[46] Similarly, the six-carbon ring of the 3,5-di-*tert*-butylcatecholate ligands in **1a**−**c** shows no evidence for the double-bond localization that is expected for an oxidized catecholate. Tetrachlorocatecholate ligands typically show shorter C−O bond distances than 3,5-di-*tert*-butylcatecholate, and in the case of nickel complexes **2a**−**c**, the observed C−O bond distances are consistent with those observed for other coordination complexes containing tetrachlorocatecholate in the fully reduced form.[47] Within the diimine ligands of complexes **1a**−**b**, **2a**−**b**, and **3a**−**b**, C=N distances of 1.30 Å are consistent with formal double bonds, and the backbone C−C distances of 1.46−1.48 Å are consistent with single bonds between sp^2-hybridized carbon atoms. In the case of (catecholate)Ni(pdi) complexes **1**−**3c**, longer C=N distances of 1.31−1.35 Å are observed. While longer C=N bonds can be indicative of the diimino-semiquinonate oxidation state (typically 1.33−1.35 Å),[48,49] the higher degree of conjugation associated with the phenanthrenediimine backbone may result in delocalization of the π-bonds over the ligand resulting in the slightly elongated C=N bond. Overall, the crystallographic data are consistent with the formal assignment of nickel(II) ions coordinated to one dianionic catecholate ligand and one neutral diimine ligand.

Solution NMR spectroscopic data for donor−acceptor complexes **1**−**3** are consistent with the observed solid-state structures and are indicative of closed-shell, square-planar nickel(II) complexes. Complexes **1**−**3** all show sharp ^{1}H NMR spectra in the normal diamagnetic region when dissolved in $CDCl_3$ or d_8-THF. According to the solid-state structures, complexes **1a**−**c**, containing the 3,5-di-*tert*-butylcatecholate donor ligand, are nominally C_s symmetric. In solution, only the (cat-tBu$_2$)Ni(bdi) derivative, complex **1a**, showed evidence for C_s symmetry, displaying two backbone methyl group resonances for the bdi acceptor ligand at 1.56 and 1.64 ppm in the ^{1}H NMR spectrum. In the case of complexes **1b** and **1c**, the acceptor ligands appear symmetric in the ^{1}H NMR spectrum, even at 500 MHz. We attribute this apparent symmetry in the NMR spectra of **1b** and **1c** to the negligible chemical environment difference imposed by the remote *tert*-butyl groups of the 3,5-di-*tert*-butylcatecholate ligand and not to fluxionality in the molecules that would average the inequivalent positions within the diimine ligand. Tetrachlorocatecholate and phenanthrenediolate complexes **2a**−**c** and **3a**-**c**, respectively, have nominal C_{2v} symmetry according to the solid-state structures, and, congruently, these complexes all show symmetric environments for the diimine acceptor ligands by solution ^{1}H NMR spectroscopy.

Electronic Spectroscopy. Nickel complexes **1**−**3** are highly colored both in the solid state and in solution, reflecting strong absorptive properties in the UV−vis−NIR regions of the electromagnetic spectrum. Figure 2 shows the absorption spectra of complexes **1**−**3** collected as solutions in THF at 298 K. Both the identity of the catecholate ligand and the diimine ligand have a strong impact on the energy and intensity of the

dx.doi.org/10.1021/ic5017214 | Inorg. Chem. 2014, 53, 8825−8837

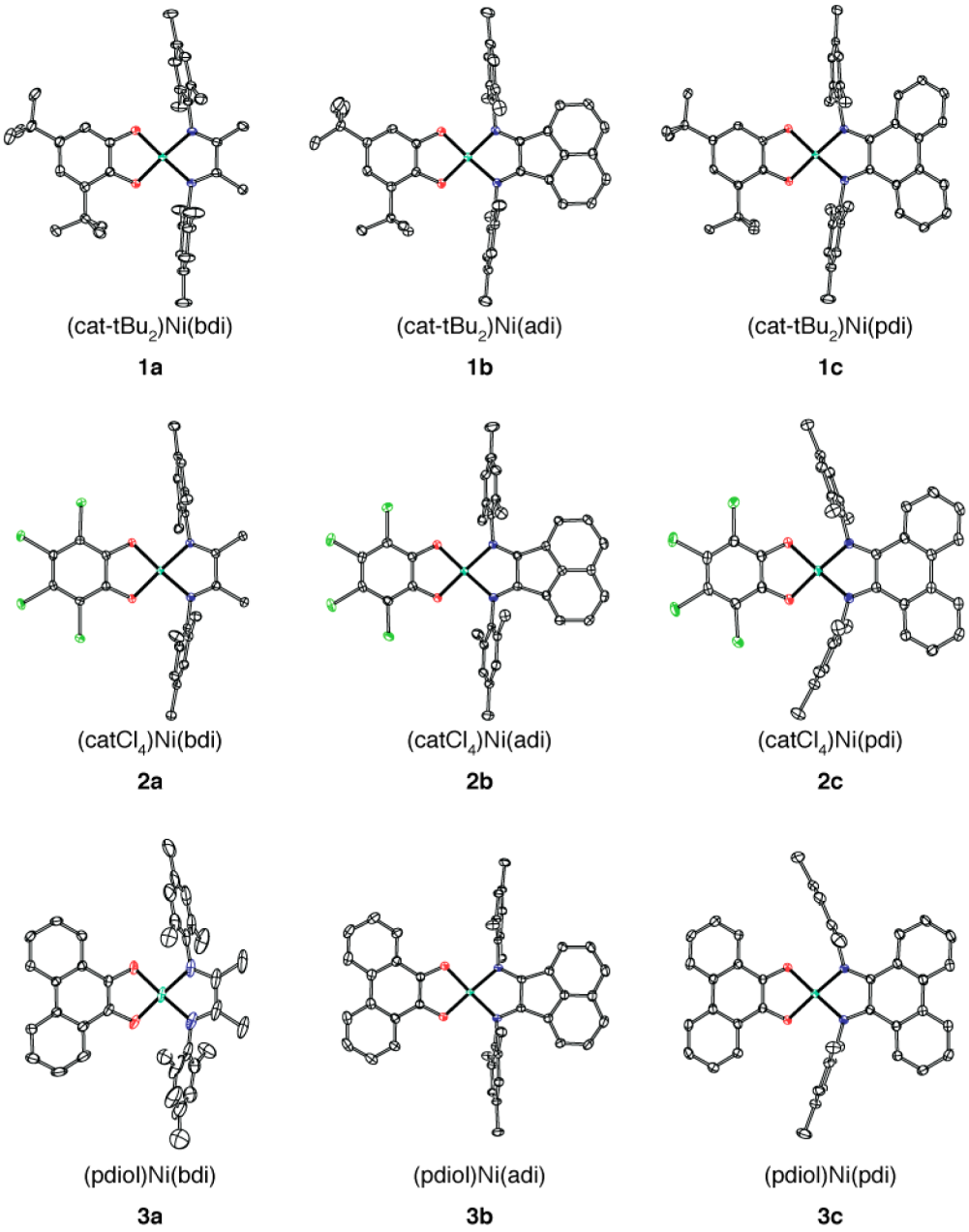

Figure 1. ORTEP diagrams of nickel(II) donor–acceptor complexes **1**–**3**. Ellipsoids are drawn at 50% probability. Hydrogen atoms and solvent molecules (if present) have been omitted for clarity.

low-energy absorption bands. As shown in Figure 2a, 3,5-di-*tert*-butylcatecholate complexes **1a**–**c** are characterized by strong absorptions throughout the visible and near-IR portions of the spectrum that red-shift as the diimine is changed from bdi to adi to pdi. There is a concomitant increase in the extinction coefficient as the absorption energy shifts to lower energy. For example, (cat-tBu$_2$)Ni(bdi), **1a**, has an absorption maximum at 816 nm (1.85 eV) with an extinction coefficient of 6510 M^{-1} cm^{-1}. In the case of (cat-tBu$_2$)Ni(adi), **1b**, the low-energy absorption is shifted to 1109 nm (1.12 eV) with an extinction coefficient of 13 300 M^{-1} cm^{-1}, whereas for (cat-tBu$_2$)Ni(pdi), **1c**, the low-energy absorption is shifted to 1186 nm (1.05 eV) with an extinction coefficient of 16 500 M^{-1} cm^{-1}. Figures 2b and 2c shows analogous trends in both the absorption energies and the intensities accompanying changes to the diimine acceptor ligand for nickel complexes of the tetrachlorocatecholate donor ligand (Figure 2b, complexes **2a**–**c**) and the phenanthrenediolate donor ligand (Figure 2c, complexes **3a**–**c**).

Comparing the absorption spectra across Figure 2a–c illustrates the impact of different catecholate ligands on the low-energy absorption feature. For a given diimine ligand, the energy of the primary absorption feature changes according to the trend tetrachlorocatecholate > 3,5-di-*tert*-butylcatecholate > phenanthrenediolate. Consider complexes **1a**, **2a**, and **3a**, which all contain the same bdi acceptor ligand. For complex **2a** containing the tetrachlorocatecholate donor ligand, the low-energy absorption is blue-shifted by 0.35 eV as compared to complex **1a** containing the di-*tert*-butylcatecholate donor ligand. Similarly, for complex **3a** containing the phenanthrenediolate donor ligand, the low-energy absorption is red-shifted by 0.71 eV as compared to complex **1a** containing the di-*tert*-

dx.doi.org/10.1021/ic5017214 | *Inorg. Chem.* 2014, 53, 8825–8837

Table 1. Selected Bond Distances (Å) for Nickel(II) Donor−Acceptor Complexes 1−3

	bond distances/Å								
	1a	1b	1c	2a	2b	2c	3a	3b	3c
Ni−O_1	1.8184(11)	1.8096(12)	1.8187(13)	1.8358(9)	1.8331(10)	1.8431(13)	1.8274(17)	1.8219(11)	1.8328(11)
Ni−O_2	1.8101(11)	1.8076(13)	1.8091(13)	1.8322(9)	1.8299(10)	1.8319(13)	1.8279(19)		1.8388(11)
Ni−N_1	1.8703(14)	1.8762(15)	1.8419(15)	1.8694(11)	1.8996(12)	1.8551(15)	1.864(2)	1.8837(13)	1.8391(13)
Ni−N_2	1.8617(14)	1.8987(15)	1.8554(16)	1.8728(11)	1.9044(12)	1.8538(15)	1.875(2)		1.8415(13)
O_1−C_1	1.350(2)	1.356(2)	1.351(2)	1.3313(16)	1.3386(16)	1.336(2)	1.347(3)	1.3441(19)	1.3282(19)
O_2−C_2	1.3535(19)	1.362(2)	1.348(2)	1.3291(15)	1.3309(18)	1.333(2)	1.347(3)		1.3297(18)
C_1−C_2	1.404(2)	1.402(2)	1.399(3)	1.4184(18)	1.412(2)	1.405(3)	1.367(3)	1.378(3)	1.384(2)
C_2−C_3	1.405(2)	1.400(2)	1.409(2)	1.3875(18)	1.391(2)	1.388(3)	1.425(3)		1.432(2)
C_3−C_4	1.402(2)	1.401(2)	1.398(3)	1.4028(18)	1.401(2)	1.395(3)	1.422(3)		1.422(2)
C_4−C_5	1.401(3)	1.399(3)	1.408(3)	1.3903(19)	1.386(2)	1.386(3)	1.456(3)	1.456(4)	1.466(2)
C_5−C_6	1.398(3)	1.395(3)	1.392(3)	1.4048(18)	1.402(2)	1.403(3)	1.421(3)	1.419(2)	1.422(2)
C_1−C_6	1.390(2)	1.385(2)	1.389(3)	1.3889(18)	1.386(2)	1.387(3)	1.429(3)	1.432(2)	1.434(2)
N_1−C_7	1.295(2)	1.299(2)	1.326(2)	1.2961(17)	1.2936(19)	1.314(2)	1.304(3)	1.302(2)	1.332(2)
N_2−C_8	1.299(2)	1.297(2)	1.321(2)	1.3010(17)	1.2906(18)	1.310(2)	1.301(4)		1.329(2)
C_7−C_8	1.474(2)	1.472(2)	1.457(2)	1.4871(18)	1.4803(19)	1.485(2)	1.462(5)	1.461(3)	1.462(2)

butylcatecholate donor ligand. This trend holds across all three diimine acceptor complexes. The strong dependence of the low-energy absorption feature on the identity of the two chelating ligands enables assignment of this band as an LL′CT transition, corresponding to the photon-induced transfer of an electron from the catecholate donor to the α-diimine acceptor. Furthermore, the position of the LL′CT transition can be tuned over broad energy ranges by changes either to the catecholate donor ligand or to the diimine acceptor ligand.

The spectra presented in Figure 2 show evidence for a vibrational progression throughout the LL′CT band. In the case of 3,5-di-*tert*-butylcatecholate and phenanthrenediolate complexes **1a−c** and **3a−c**, respectively, the vibrational progression is partially resolved at room temperature with an estimated band spacing in the range of 1200−1500 cm^{-1}. In the case of tetrachlorocatecholate complexes **2a−c**, individual bands of the vibrational progression are not resolved; however, distinct non-Gaussian band shapes are evident, especially in the spectrum of **2c**. Interestingly, the dominant vibrational transition seems to change as the charge-transfer band shifts to lower energy. As shown in Figure 2a, the most intense absorption for complex **1a** appears to be the $\nu_0 \rightarrow \nu_1'$ transition at 816 nm with the lower intensity and lower energy $\nu_0 \rightarrow \nu_0'$ transition appearing at approximately 940 nm. In the case of complex **1b**, the $\nu_0 \rightarrow \nu_0'$ transition is most intense at 1109 nm with the $\nu_0 \rightarrow \nu_1'$ transition at approximately 960 nm having lower intensity. Similar trends in the dominant vibrational transition can be observed in Figures 2b and 2c corresponding to complexes **2a−c** and **3a−c**, respectively.

The position of the LL′CT electronic absorption band of complexes **1−3** shows a strong solvent dependence. Figure 3a shows the UV−vis−NIR absorption spectrum of (cat-tBu$_2$)Ni(bdi) (**1a**) in a series of organic solvents (toluene, benzene, THF, CH_2Cl_2, DMF, and MeCN). In general, the LL′CT band shifts to lower energy with decreasing solvent polarity. The vibrational progression within the LL′CT transition becomes more pronounced in less polar solvents. It is again clear that the strongest vibronic transition changes as the charge-transfer band shifts to lower energy.

The magnitude of the solvent-dependent shift of the charge-transfer band is shown graphically in Figure 3b where the energy of the absorption band is plotted as a function of the empirical solvent number (ESN) as defined by Eisenberg and co-workers for platinum diimine dithiolate complexes.[22] To eliminate errors associated with changes in the intensity of different vibronic bands, the excited-state energies used in Figure 3b were estimated from the low-energy onset of the absorption curve (see the Supporting Information). The slope of the line in Figure 3b gave a solvatochromic shift of 0.23 for **1a**. Absorption spectra in various solvents were collected for all nine complexes to determine the solvatochromic shift values across the three donor ligands and the three acceptor ligands (Table 2). In general, the higher-energy charge-transfer bands show a more pronounced solvent dependence than those shifted to lower energy.

Electrochemistry. To further probe the electronic properties of complexes **1−3**, cyclic voltammetric studies were carried out. Figure 4 shows the cyclic voltammetry data for **1−3** in THF solutions containing 100 mM [Bu_4N][PF_6] as the supporting electrolyte. Four electrochemical events are obvious in the cyclic voltammogram for each complex, comprising two one-electron reductions and two one-electron oxidations. In every case, both reductions are reversible ($i_{pa}/i_{pc} \cong 1.0$), as is the first oxidation event. The second oxidation of complexes **1−3** shows at least partial reversibility. Reduction potentials for **1−3** are collected in Table 3.

The difference between the potentials of the first reduction and the first oxidation for **1−3** provides an estimate of the equilibrium HOMO-LUMO gap.[7,22]The potential of the first reduction ($E^{\circ\prime}{}_3$) demonstrated a strong dependence on the α-diimine ligand, with the butanediimine derivatives being the most difficult to reduce and the phenanthrenediimine derivatives being the easiest to reduce. Similarly, changing the catecholate ligand resulted in appreciable changes to the potential of the first oxidation ($E^{\circ\prime}{}_2$). The tetrachlorocatecholate complexes are more difficult to oxidize than the 3,5-di-*tert*-butylcatecholate congeners, which in turn are more difficult to oxidize than the phenanthrenediolate complexes.

Chemical Oxidation and Reduction of 1b. To gain further insight into the loci of the oxidative and reductive processes in **1−3**, chemical oxidation and reduction reactions were investigated. On the basis of the cyclic voltammetry data, complex **1b**, (cat-tBu$_2$)Ni(adi), is best suited for chemical oxidation and reduction studies as it has well-resolved, one-electron oxidation and reduction processes at modest potentials.

dx.doi.org/10.1021/ic5017214 | Inorg. Chem. 2014, 53, 8825−8837

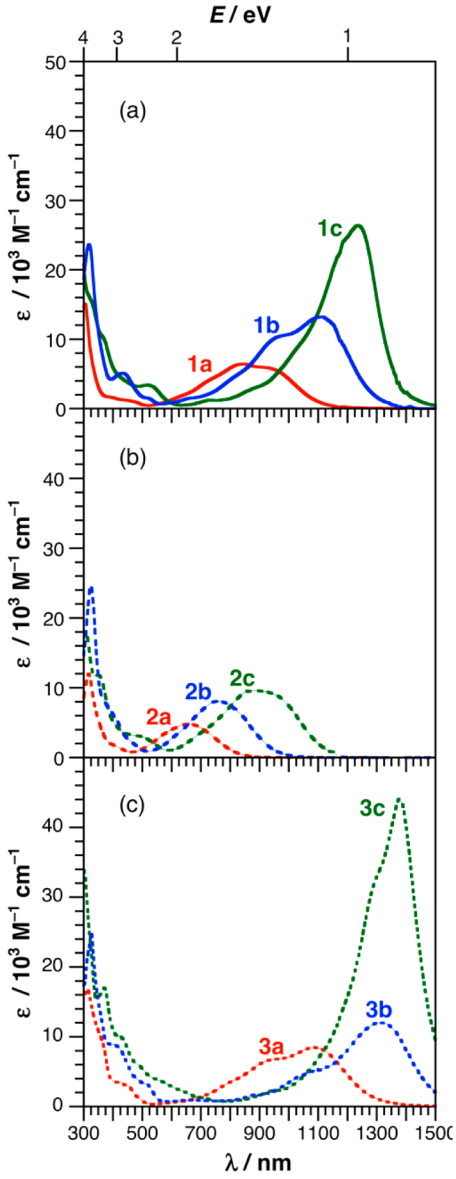

Figure 2. Solution UV−vis−NIR absorption spectra of (a) (cat-tBu$_2$)Ni(diimine) complexes **1a**−**c**, (b) (catCl$_4$)Ni(diimine) complexes **2a**−**c**, and (c) (pdiol)Ni(diimine) complexes **3a**−**c** in THF at 298 K.

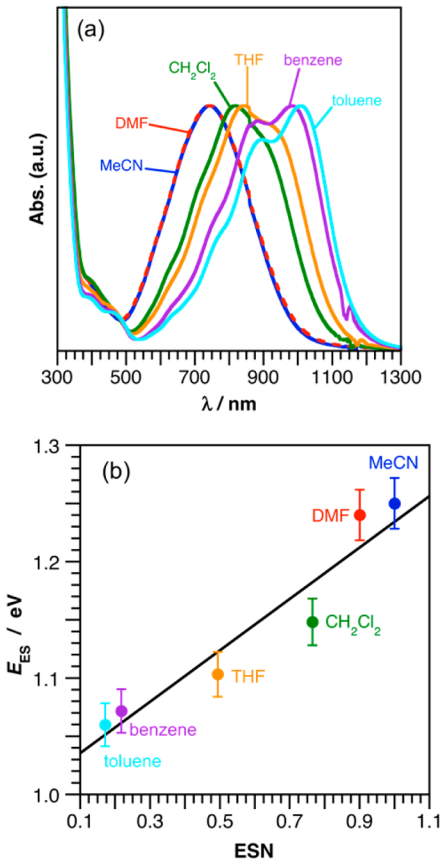

Figure 3. (a) Normalized UV−vis−NIR absorption spectra of **1a** in toluene, benzene, THF, CH_2Cl_2, DMF, and MeCN, and (b) plot of the estimated excited-state energy for **1a** versus the empirical solvent number[22] for each solvent.

Table 2. Absorption Maxima in THF (nm), Estimated Low-Energy Onset of the Absorption Band in THF (eV), and Solvatochromic Shifts Associated with the Low-Energy Absorption Band of Nickel Complexes 1−3

	abs λ_{max}/nm	estimated E_{LLCT}/eV	solvatochromic shift
1a	884	1.12	0.23
1b	1108	0.96	0.13
1c	1236	0.91	0.02
2a	658	1.50	0.19
2b	758	1.29	0.28
2c	882	1.10	0.19
3a	1090	0.96	0.17
3b	1310	0.821	0.07
3c	1370	0.823	0

One-electron oxidation of **1b** affords a cationic complex with the locus of oxidation at the catecholate ligand. Treatment of an acetonitrile solution of **1b** with solid AgOTf at ambient temperature resulted in a color change from dark green to brown with concomitant deposition of a dark solid. The product, [(cat-tBu$_2$)Ni(adi)][OTf], [**1b**][OTf], was isolated as an amorphous solid. As expected, the product cation, [**1b**]$^+$, is paramagnetic and attempts to acquire NMR spectra were unsuccessful; however, it was readily characterized as an S = 1/2 species by EPR spectroscopy at both 298 and 77 K. Figure 5a shows the X-band EPR spectrum of [**1b**]$^+$ in CH_2Cl_2 at 298 K. An isotropic signal centered at g = 2.0071 is characteristic of a semiquinonate radical, and similar EPR spectra have been reported for semiquinonate complexes of square-planar nickel. The spectrum was fit by assuming coupling to a single semiquinonate proton (a_H = 4 G) at the 4-position of the aryl ring. Cooling the EPR sample of [**1b**]$^+$ to 77 K resulted in a broadening of the EPR signal into the baseline.

One-electron reduction of **1b** was readily achieved using decamethylcobaltocene (Cp*$_2$Co). The reduction product, [Cp*$_2$Co][(cat-tBu$_2$)Ni(adi)], [Cp*$_2$Co][**1b**], was isolated as a green, amorphous solid. Again, the S = 1/2 species is not NMR active, but it was readily characterized by EPR spectroscopy. Figure 5b shows the 77 K EPR spectrum of [**1b**]$^-$ in a mixture of MeCN and toluene. The axial signal gave $g_{\|}$ = 2.0286 and $g_{\perp}$ = 2.0035 and was fit with a hyperfine interaction to the two nitrogen atoms of the adi ligand (avg a_N = 24 G).

dx.doi.org/10.1021/ic5017214 | Inorg. Chem. 2014, 53, 8825−8837

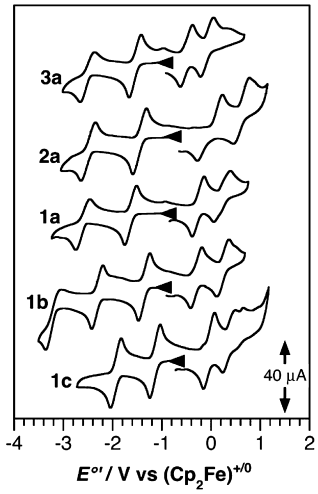

Figure 4. Cyclic voltammetry plots for complexes **1a–c**, **2a**, and **3a**. Data were collected at 298 K in THF solutions that were 1.0 mM in analyte and 0.1 M in $[Bu_4N][PF_6]$ electrolyte using a glassy carbon working electrode. All potentials were referenced to $[Cp_2Fe]^{+/0}$ using an internal standard.

Table 3. Reduction Potentials (V vs $[Cp_2Fe]^{+/0}$) for Complexes 1–3 at 298 K in THF Solution

	$E^{\circ\prime}$/V vs $[Cp_2Fe]^{+/0}$				
	$E^{\circ\prime}{}_1$ $[Ni]^{2+/1+}$	$E^{\circ\prime}{}_2$ $[Ni]^{1+/0}$	$E^{\circ\prime}{}_3$ $[Ni]^{0/1-}$	$E^{\circ\prime}{}_4$ $[Ni]^{1-/2-}$	$E^{\circ\prime}{}_2 - E^{\circ\prime}{}_3$
1a	0.16	−0.27	−1.65	−2.58	1.38
1b	0.17	−0.33	−1.40	−2.34	1.07
1c	0.47	−0.16	−1.28	−2.10	1.12
2a	0.67	0.20	−1.35	−2.41	1.55
2b	0.58	−0.15	−1.21	−2.18	1.06
2c	0.63	0.29	−0.95	−1.82	1.24
3a	−0.15	−0.55	−1.57	−2.52	1.02
3b	−0.13	−0.63	−1.33	−2.24	0.70
3c	−0.04	−0.27	−1.19	−1.95	0.92

Both the cation, $[\mathbf{1b}]^+$, and the anion, $[\mathbf{1b}]^-$, have markedly different absorption profiles from the neutral donor–acceptor complex **1b**. Figure 6 shows an overlay of the UV–vis–NIR absorption spectra for $[\mathbf{1b}]^+$, **1b**, and $[\mathbf{1b}]^-$. Oxidation of **1b** to form the cation $[\mathbf{1b}]^+$ virtually eliminates the low-energy absorption band in the UV–vis–NIR spectrum, while the high-energy absorptions remain largely unchanged. In the anion, $[\mathbf{1b}]^-$, the low-energy absorption band is reduced in intensity and blue-shifted significantly.

DISCUSSION

Access to the catecholate and *ortho*-quinone forms of the 3,5-di-*tert*-butylcatecholate ligand provided two synthetic routes to form donor–acceptor complexes **1a–c**. Metathesis reactivity employing $(dme)NiCl_2$ and the dilithium salt of the catecholate ligand provided **1a–c** in good yields and purity. Alternatively, the nickel(0) synthon $Ni(cod)_2$ allowed complexes **1a–c** to be prepared utilizing 3,5-di-*tert*-butyl-1,2-quinone as the source of the catecholate donor ligand. In the latter reaction, the nickel(0) metal center is presumably oxidized in an inner-sphere, two-electron reaction upon coordination of the quinone to the metal center. This latter, redox reaction pathway was also convenient for the synthesis of complexes **2a–c**, using

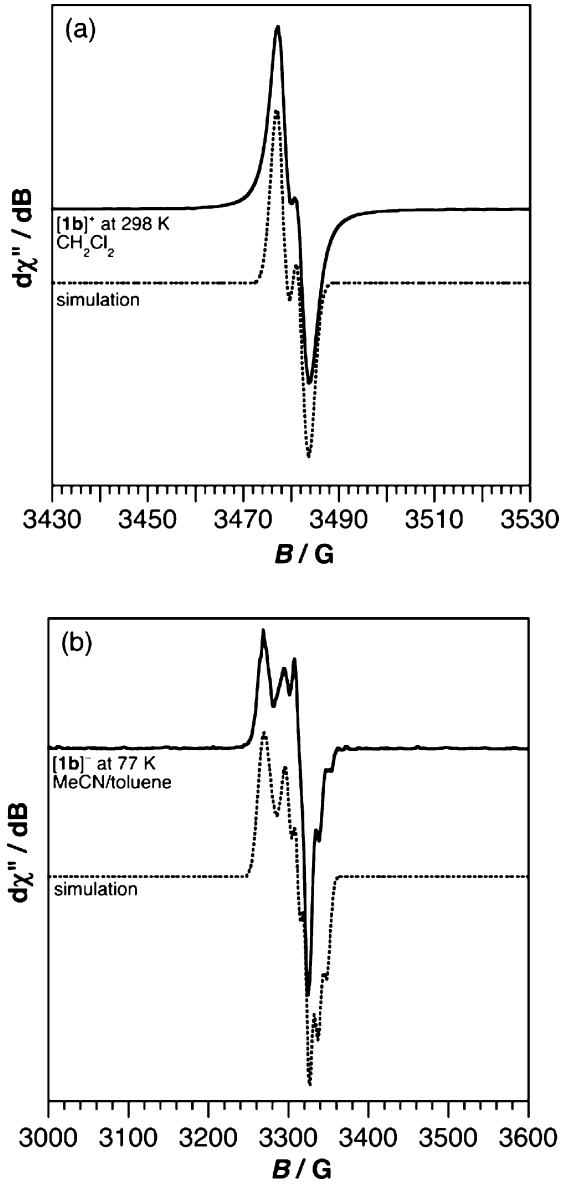

Figure 5. Experimental and simulated X-band EPR spectra of (a) $[(cat\text{-}tBu_2)Ni(adi)][OTf]$, $[\mathbf{1b}][OTf]$, in CH_2Cl_2 at 298 K, and (b) $[Cp^*_2Co][(cat\text{-}tBu_2)Ni(adi)]$, $[Cp^*_2Co][\mathbf{1b}]$, in a mixture of MeCN and toluene at 77 K.

tetrachloroquinone, and complexes **3a–c**, using 9,10-phenanthrenequinone.

Crystallographic analysis of all nine donor–acceptor complexes established both the gross structural features of the square planar, nickel(II) coordination environment as well as the subtle structural diagnostics of the catecholate donor and α-diimine acceptor ligands. As has been established for square planar complexes of other group 10 metals with redox-active ligands, the relative electronic properties of the ligands dictate the frontier electronic structure of the complex.[13,19,20,50,51] In cases where the redox-active ligands are identical (homoleptic complexes), a symmetric, open-shell biradical electronic structure is preferred in which the two redox-active ligands exist in the semiquinonate oxidation state. In cases where the two redox-active ligands are significantly different, push–pull or donor–acceptor complexes put one redox-active ligand in the reduced, catecholate oxidation state and the other redox-active

dx.doi.org/10.1021/ic5017214 | Inorg. Chem. 2014, 53, 8825–8837

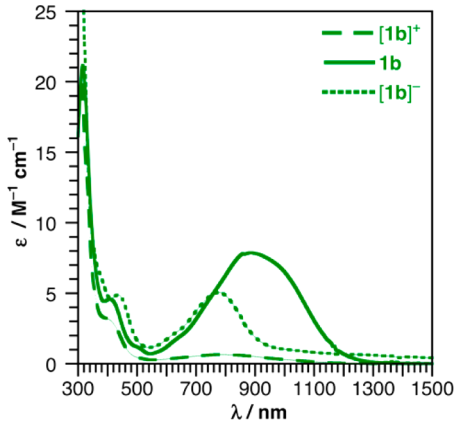

Figure 6. UV−vis−NIR absorption spectra of $[(\text{cat-}t\text{Bu}_2)\text{Ni(adi)}]^+$, $[\mathbf{1b}]^+$, $(\text{cat-}t\text{Bu}_2)\text{Ni(adi)}$, **1b**, and $[(\text{cat-}t\text{Bu}_2)\text{Ni(adi)}]^-$, $[\mathbf{1b}]^-$ in MeCN at room temperature.

ligand in the oxidized, quinone oxidation state. For complexes **1**−**3**, the high-resolution crystallographic data indicate that these complexes fall into the latter category: in every case, the best description of the complex has a fully reduced catecholate donor ligand and a fully oxidized α-diimine acceptor ligand.

Further support for the primacy of the ligand frontier orbitals was obtained from the EPR spectra for $[\mathbf{1b}]^+$ and $[\mathbf{1b}]^-$. The cation, $[\mathbf{1b}]^+$, was characterized by an isotropic EPR spectrum at room temperature with hyperfine coupling to a single semiquinonate proton in the 4 position. Hyperfine coupling to the proton in the 6 position is not observed, consistent with removal of a single electron from the catecholate HOMO, as that π orbital has a node at the 3 and 6 positions of the benzene ring. In the anion, $[\mathbf{1b}]^-$, an axial EPR signal was observed and fit by assuming coupling to the nitrogen atoms of the adi acceptor ligand. The magnitude of the nitrogen hyperfine coupling constant at 24 G is roughly one-half of the value obtained from EPR spectra of sodium salts of the adi radical anion,[52] suggesting that the unpaired electron in $[\mathbf{1b}]^-$ is delocalized onto the nickel center. The axial shape of the EPR spectrum for $[\mathbf{1b}]^-$ is also consistent with this postulate. The qualitative molecular orbital diagram displayed in Figure 7 illustrates why the EPR spectrum for anion $[\mathbf{1b}]^-$ shows evidence for delocalization of the unpaired electron onto the nickel center, whereas the spectrum of the cation $[\mathbf{1b}]^+$ does

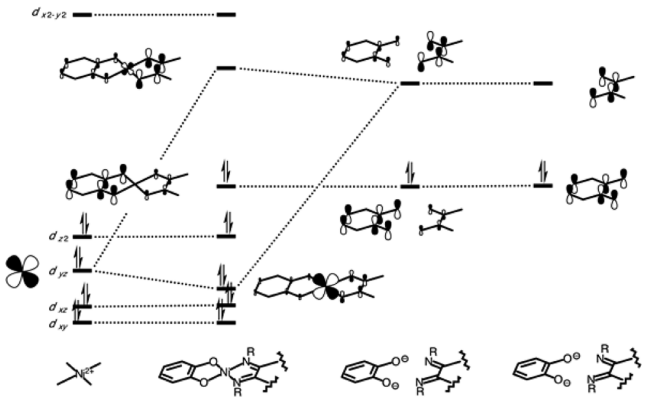

Figure 7. Simplified molecular orbital diagram highlighting the interaction of the redox-active ligand orbitals with the nickel d_{yz} orbital.

not. Assuming idealized C_{2v} symmetry, the redox-active donor orbital of the catecholate and the redox-active acceptor orbital of the diimine both have b_2 symmetry. Mixing of these ligand orbitals leads to in-phase and out-of-phase combinations that interact with the b_2-symmetric, d_{yz} orbital of the nickel. In this case, the nickel d_{yz} orbital only has a net interaction with the out-of-phase combination that is localized on the diimine acceptor ligand, leaving the in-phase combination, which is localized on the catecholate donor, as a pure ligand-based orbital.

Juxtaposition of a catecholate donor ligand and a diimine acceptor ligand on a square planar nickel(II) center affords low-energy charge-transfer absorptions in the electronic spectrum. On the basis of the spectroscopic data obtained for **1**−**3**, the low-energy absorption bands have been assigned as LL′CT transitions, corresponding to the transfer of an electron from the catecholate donor ligand to the α-diimine acceptor ligand. For nickel complexes **1**−**3**, the contracted nature of the metal 3d orbitals and hard character of the catecholate oxygen donor atoms result in less metal character in the charge-transfer transition than has been observed for related platinum dithiolates and bis(acetylide) complexes.[22] Nevertheless, the LL′CT band for complexes **1**−**3** is sensitive to the solvent polarity, with solvatochromic shifts similar to the values determined for the platinum complexes studied by Eisenberg and co-workers.[22] This type of negative solvatochromic shift has been attributed to a charge-transfer transition from a dipolar ground state to a nonpolar excited state, and is entirely consistent with a donor−acceptor ground state arising from a catecholate donor ligand and an α-diimine acceptor ligand. In general, the magnitude of the solvatochromic shift appears to correlate with the energy of the LL′CT absorption band. Specifically, the higher-energy LL′CT absorptions of **2a**−**c** are more sensitive to the solvent polarity than the lower-energy LL′CT absorptions of **3a**−**c** (with the sensitivity of **1a**−**c** falling in the middle). Within the context of Figure 7, this trend in the solvatochromic shift is an indicator of the degree of mixing between the catecholate donor and α-diimine acceptor orbitals. In **2a**−**c**, the energy separation between the tetrachlorocatecholate HOMO and the α-diimine LUMO is large, leading to very little orbital mixing. The resultant dipolar ground state manifests a LL′CT transition that is highly sensitive to solvent polarity. In **3a**−**c**, the energy separation between the 9,10-phenanthrenediolate HOMO and the α-diimine LUMO is small, allowing significant orbital mixing. In this case, the ground state is less dipolar and the absorption band takes on significant π to π^* character, which is less sensitive to solvent polarity.

Consistent with the LL′CT assignment for the low-energy absorption features of **1**−**3**, the energies of these transitions correlate with the HOMO−LUMO gap determined by electrochemical experiments.[7,22,53−55] Figure 8 shows a plot of the LL′CT transition energy versus the HOMO−LUMO gap as determined by electrochemistry ($E_2^{\circ\prime} - E_3^{\circ\prime}$). For the energy of the LL′CT transition, the absorption onset energy (as described in the Supporting Information) was used to avoid the introduction of error due to the vibrational progression evident in the absorption bands. The optical and electrochemical measures of the HOMO−LUMO gap show a strong correlation with the exception of the three complexes containing the adi acceptor ligand, **1b**, **2b**, and **3b**, shown in blue in Figure 8. These three complexes are shifted significantly from their closest counterparts. Thus, **2b** shows a small electrochemical

dx.doi.org/10.1021/ic5017214 | Inorg. Chem. 2014, 53, 8825−8837

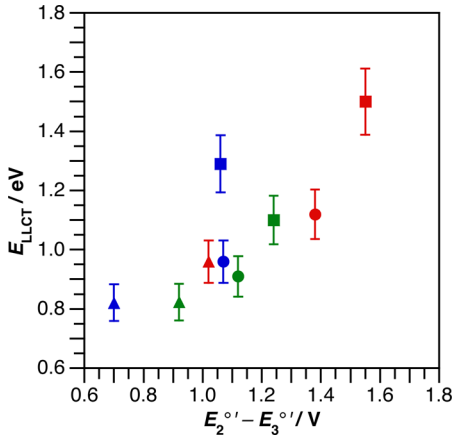

Figure 8. Plot of the LLCT energy (eV) in THF versus the electrochemical HOMO–LUMO gap (V) for **1a–c** (●), **2a–c** (■), and **3a–c** (▲). The electrochemical HOMO–LUMO gap was calculated as the difference between the potentials for first electrochemical oxidation and the first electrochemical reduction, $E_2^{o\prime} - E_3^{o\prime}$, in THF.

HOMO–LUMO gap as compared to $(catCl_4)^{2-}$ counterparts **2a** and **2c**. A similar discrepancy is evident for **1b** relative to **1a** and **1c** and for **3b** relative to **3a** and **3c**. The genesis of this discrepancy may be found in the electrochemical data of Table 3. To a first approximation, the electrochemical potentials for the first reduction follow the expected trend based on acceptor ligand (bdi < adi < pdi), whereas the electrochemical potentials for the first oxidation follow the expected trend based on the acceptor ligand ($pdiol^{2-}$ < cat-tBu_2^{2-} < $catCl_4^{2-}$). In general, we would expect the donor ligand to have a minor effect on the potential of the first reduction and the acceptor ligand to have a minor effect on the potential of the first oxidation. In the case of the adi acceptor ligand, this latter expectation is not met. For **1b**, **2b**, and **3b**, the adi ligand has a pronounced effect on the potential of the first oxidation, and as such, the adi derivatives are the easiest to oxidize for a given catecholate donor ligand. Thus, **1b** is easier to oxidize that **1a** or **1c**, **2b** is easier to oxidize than **2a** or **2c**, and **3b** is easier to oxidize than **3a** or **3c**. The cathodic shift in the $E_2^{o\prime}$ values for **1b**, **2b**, and **3b** in THF suggests that the adi ligand is better able to stabilize the cationic form of the nickel complex, which could be a manifestation of stronger σ-donor ability of adi compared to other α-diimine ligands. Because the diimine ligands affect the first reduction and first oxidation differently, the electrochemical measurement of the HOMO–LUMO gap ends up being smaller than expected for adi complexes **1b**, **2b**, and **3c**.

■ CONCLUSIONS

The new family of nickel donor–acceptor complexes reported herein represents an attractive type of charge-transfer dye complex with potential applications in solar energy conversion schemes and electron-transfer photochemistry. These dyes have several attractive features, including the incorporation of an earth-abundant metal and readily available ligands rather than precious metals and designer ligand platforms. Most significantly, the modular construction of these dyes leads to attractive electronic features including broadly tunable absorption characteristics and electrochemical parameters. Because the dye HOMO is localized on the catecholate ligand and the dye LUMO is localized on the α-diimine ligand and because these ligands are installed independently, the optical and electrochemical properties of these dyes can be tuned semi-independently. Table 4 summarizes the estimated excited-state redox potentials for complexes **1–3** based on the absorption data of Table 2 and the electrochemical data of Table 3 (converted to the SCE scale by assuming a formal potential for $[Cp_2Fe]^{+/0}$ of +0.56 V vs SCE).[32] Strong excited-state reductants are accessible with highly red-shifted absorption profiles. For example, (pdiol)Ni(bdi) (**3a**) is estimated to be an excited-state reductant that is comparable to $[Ru(bpy)_3]^{2+}$ ($E^{+/*}$ is −0.8 V vs SCE for the ^{3}MLCT state and −1.2 V vs SCE for the ^{1}MLCT state).[7] Whereas $[Ru(bpy)_3]^{2+}$ requires a 2.5 eV photon to access the excited state, **3a** accesses the excited state upon absorption of a 1 eV photon. In the case of **3a**, the strongly reducing 9,10-phenanthrenediolate donor ligand enables the red-shift of the charge-transfer absorption. LL′CT dyes **2a–c**, with the less electron-rich donor ligand $(catCl_4)^{2-}$, can be modest excited-state oxidants, with estimated $E^{*/-}$ values of up to +0.70 V vs SCE. While these potentials fall short of the $E^{*/-}$ value for $[Ru(bpy)_3]^{2+}$ ($E^{*/-}$ = +1.2 V vs SCE),[7] several factors suggest that dyes analogous to those reported here could meet and possibly exceed the performance of the ruthenium dyes as an excited-state oxidant. For example, **2c** is estimated to have an $E^{*/-}$ of 0.69 V vs SCE upon absorption of a 1.1 eV photon. Incorporation of a less electron-rich donor ligand (e.g., $catF_4^{2-}$) would be expected to lower the HOMO energy without significant change to the LUMO localized on the acceptor ligand. Thus, the LL′CT absorption would shift to higher energy and generate a stronger excited-state oxidant. This strategy has been nicely illustrated in a family of dirhodium LL′CT dyes, which manifest excited-state oxidation potentials as high as +1.4 V vs SCE.[56] A second factor to consider is that the hole generated upon excitation of $[Ru(bpy)_3]^{2+}$ is localized on the ruthenium center and is "protected" by the bipyridal ligands, leading to slow hole extraction kinetics.[57] In the case of complexes **1–3**, excitation leads to the formation of a hole on the donor ligand itself, which should lead to faster hole transfer in schemes applying these dyes as excited-state oxidants.

The electronic properties of the new donor–acceptor LL′CT dye reported herein make them excellent candidates for investigation as the sensitizers in dye-sensitized solar cells (DSSCs).[58,59] In particular, the broad electronic tunability of these dyes and their potential to act as either excited-state

Table 4. Estimated Excited-State Redox Potentials (V vs SCE) for Complexes 1–3

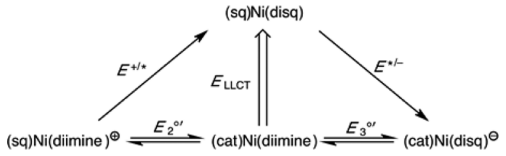

	$E^{+/*}$/V vs SCE	$E^{*/-}$/V vs SCE
1a	−0.82	0.02
1b	−0.72	0.11
1c	−0.50	0.18
2a	−0.73	0.70
2b	−0.87	0.63
2c	−0.23	0.69
3a	−0.94	−0.06
3b	−0.90	0.06
3c	−0.53	0.19

dx.doi.org/10.1021/ic5017214 | Inorg. Chem. 2014, 53, 8825–8837

reductants or oxidants make them ideal candidates for use in tandem DSSCs for photoelectrolysis. Efficient tandem DSSC designs of this type will require the use of multiple charge-transfer dyes that have complementary absorption profiles in the visible and near-IR portions of the electromagnetic spectrum.[60,61] The design of dyes **1**−**3** is poised to meet that requirement. To evaluate further the application of the dyes to tandem DSSCs, new synthetic efforts must drive toward the development of molecular dyes that include covalent linkages for binding to semiconductor surfaces. Hole-injecting dyes must be anchored through the catecholate donor ligand, while electron-injecting dyes must be anchored through the acceptor ligand. Furthermore, the excited-state dynamics of these donor−acceptor LL′CT dyes must be examined to derive lifetimes for the charge separated state as well as the rates of electron and hole injection upon attachment to semiconductor surfaces. These experiments are currently underway.

■ ASSOCIATED CONTENT

Ⓢ Supporting Information

Details concerning X-ray crystallography (including cif files), UV−vis−NIR spectroscopy, and electrochemical analyses. This material is available free of charge via the Internet at http://pubs.acs.org.

■ AUTHOR INFORMATION

Corresponding Author

*E-mail: aheyduk@uci.edu.

Notes

The authors declare no competing financial interest.

■ ACKNOWLEDGMENTS

Financial support for this research was provided by The Research Corporation for Science Advancement Scialog: Solar Energy Conversion and the UCI Physical Sciences Center for Solar Energy.

■ REFERENCES

(1) Wasielewski, M. R. *Chem. Rev.* **1992**, *92*, 435−461.
(2) Gust, D.; Moore, T. A.; Moore, A. L. *Acc. Chem. Res.* **2001**, *34*, 40−48.
(3) Gust, D.; Moore, T. A.; Moore, A. L. *Acc. Chem. Res.* **2009**, *42*, 1890−1898.
(4) Wasielewski, M. R. *Acc. Chem. Res.* **2009**, *42*, 1910−1921.
(5) Campagna, S.; Puntoriero, F.; Nastasi, F.; Bergamini, G.; Balzani, V. *Top. Curr. Chem.* **2007**, *280*, 117−214.
(6) Balzani, V.; Barigelletti, F.; De Cola, L. *Top. Curr. Chem.* **1990**, 31−71.
(7) Juris, A.; Balzani, V.; Barigelletti, F.; Campagna, S.; Belser, P. L.; Von Zelewsky, A. *Coord. Chem. Rev.* **1988**, *84*, 85−277.
(8) McCusker, J. K. *Acc. Chem. Res.* **2003**, *36*, 876−887.
(9) Masui, H.; Lever, A. B. P.; Auburn, P. R. *Inorg. Chem.* **1991**, *30*, 2402−2410.
(10) Chaudhuri, P.; Verani, C. N.; Bill, E.; Bothe, E.; Weyhermüller, T.; Wieghardt, K. *J. Am. Chem. Soc.* **2001**, *123*, 2213−2223.
(11) Herebian, D.; Bothe, E.; Bill, E.; Weyhermüller, T.; Wieghardt, K. *J. Am. Chem. Soc.* **2001**, *123*, 10012−10023.
(12) Bachler, V.; Olbrich, G.; Neese, F.; Wieghardt, K. *Inorg. Chem.* **2002**, *41*, 4179−4193.
(13) Herebian, D.; Bothe, E.; Neese, F.; Weyhermüller, T.; Wieghardt, K. *J. Am. Chem. Soc.* **2003**, *125*, 9116−9128.
(14) Kokatam, S.; Weyhermüller, T.; Bothe, E.; Chaudhuri, P.; Wieghardt, K. *Inorg. Chem.* **2005**, *44*, 3709−3717.
(15) Ray, K.; Weyhermuller, T.; Neese, F.; Wieghardt, K. *Inorg. Chem.* **2005**, *44*, 5345−5360.
(16) Schrauzer, G. N.; Mayweg, V. *J. Am. Chem. Soc.* **1962**, *84*, 3221−3221.
(17) Davison, A.; Edelstein, N.; Holm, R. H.; Maki, A. H. *J. Am. Chem. Soc.* **1963**, *85*, 2029−2030.
(18) Stiefel, E. I.; Waters, J. H.; Billig, E.; Gray, H. B. *J. Am. Chem. Soc.* **1965**, *87*, 3016−3017.
(19) Deplano, P.; Pilia, L.; Espa, D.; Mercuri, M. L.; Serpe, A. *Coord. Chem. Rev.* **2010**, *254*, 1434−1447.
(20) Garreau-de Bonneval, B.; Moineau-Chane Ching, K. I.; Alary, F.; Bui, T.-T.; Valade, L. *Coord. Chem. Rev.* **2010**, *254*, 1457−1467.
(21) Zuleta, J. A.; Bevilacqua, J. M.; Rehm, J. M.; Eisenberg, R. *Inorg. Chem.* **1992**, *31*, 1332−1337.
(22) Cummings, S. D.; Eisenberg, R. *J. Am. Chem. Soc.* **1996**, *118*, 1949−1960.
(23) Paw, W.; Cummings, S. D.; Mansour, M. A.; Connick, W. B.; Geiger, D. K.; Eisenberg, R. *Coord. Chem. Rev.* **1998**, *171*, 125−150.
(24) Connick, W. B.; Geiger, D.; Eisenberg, R. *Inorg. Chem.* **1999**, *38*, 3264−3265.
(25) Weinstein, J. A.; Tierney, M. T.; Davies, E. S.; Base, K.; Robeiro, A. A.; Grinstaff, M. W. *Inorg. Chem.* **2006**, *45*, 4544−4555.
(26) Best, J.; Sazanovich, I. V.; Adams, H.; Bennett, R. D.; Davies, E. S.; Meijer, A. J.; Towrie, M.; Tikhomirov, S. A.; Bouganov, O. V.; Ward, M. D.; Weinstein, J. A. *Inorg. Chem.* **2010**, *49*, 10041−10056.
(27) Yang, J.; Kersi, D. K.; Giles, L. J.; Stein, B. W.; Feng, C.; Tichnell, C. R.; Shultz, D. A.; Kirk, M. L. *Inorg. Chem.* **2014**.
(28) Zhong, H. A.; Labinger, J. A.; Bercaw, J. E. *J. Am. Chem. Soc.* **2002**, *124*, 1378−1399.
(29) Gasperini, M.; Ragaini, F.; Cenini, S. *Organometallics* **2002**, *21*, 2950−2957.
(30) Ketterer, N. A.; Ziller, J. W.; Rheingold, A. L.; Heyduk, A. F. *Organometallics* **2007**, *26*, 5330−5338.
(31) Stoll, S.; Schweiger, A. *J. Magn. Reson.* **2006**, *178*, 42−55.
(32) Connelly, N. G.; Geiger, W. E. *Chem. Rev.* **1996**, *96*, 877−910.
(33) Sheldrick, G. M. *SHELXTL, Version 6.12*; 2001.
(34) *International Tables for X-ray Crystallography*; Kluwer Academic: Dordrecht, Netherlands, 1992.
(35) Farrugia, L. J. *J. Appl. Crystallogr.* **1997**, *30*, 565−565.
(36) Pierpont, C. G.; Downs, H. H.; Rukavina, T. G. *J. Am. Chem. Soc.* **1974**, *96*, 5573−5574.
(37) Pierpont, C. G.; Downs, H. H. *J. Am. Chem. Soc.* **1976**, *98*, 4834−4838.
(38) Buchanan, R. M.; Downs, H. H.; Shorthill, W. B.; Pierpont, C. G.; Kessel, S. L.; Hendrickson, D. N. *J. Am. Chem. Soc.* **1978**, *100*, 4318−4320.
(39) Downs, H. H.; Buchanan, R. M.; Pierpont, C. G. *Inorg. Chem.* **1979**, *18*, 1736−1740.
(40) Sofen, S. R.; Ware, D. C.; Cooper, S. R.; Raymond, K. N. *Inorg. Chem.* **1979**, *18*, 234−239.
(41) Sgro, M. J.; Stephan, D. W. *Dalton Trans.* **2010**, *39*, 5786−5794.
(42) Bhattacharya, S.; Gupta, P.; Basuli, F.; Pierpont, C. G. *Inorg. Chem.* **2002**, *41*, 5810−5816.
(43) Rosokha, S. V.; Kochi, J. K. *Struct. Bonding (Berlin)* **2008**, *126*, 137−160.
(44) Brown, S. N. *Inorg. Chem.* **2012**, *51*, 1251−1260.
(45) Brueckner, C.; Caulder, D. L.; Raymond, K. N. *Inorg. Chem.* **1998**, *37*, 6759−6764.
(46) Abakumov, G. A.; Cherkasov, V. K.; Bubnov, M. P.; Ellert, O. G.; Rakitin, Y. V.; Zakharov, L. N.; Struchkov, Y. T.; Saf'yanov, Y. N. *Russ. Chem. Bull.* **1992**, *41*, 1813−1818.
(47) Brasse, M.; Cámpora, J.; Davies, M.; Teuma, E.; Palma, P.; Álvarez, E.; Sanz, E.; Reyes, M. *Adv. Synth. Catal.* **2007**, *349*, 2111−2120.
(48) Chlopek, K.; Bothe, E.; Neese, F.; Weyhermueller, T.; Wieghardt, K. *Inorg. Chem.* **2006**, *45*, 6298−6307.
(49) Muresan, N.; Weyhermueller, T.; Wieghardt, K. *Dalton Trans.* **2007**, 4390−4398.
(50) Fox, G. A.; Pierpont, C. G. *Inorg. Chem.* **1992**, *31*, 3718−3723.
(51) Lange, C. W.; Pierpont, C. G. *Inorg. Chim. Acta* **1997**, *263*, 219−224.

(52) Fedushkin, I. L.; Skatova, A. A.; Chudakova, V. A.; Cherkasov, V. K.; Fukin, G. K.; Lopatin, M. A. *Eur. J. Inorg. Chem.* **2004**, 388−393.
(53) Rillema, D. P.; Allen, G.; Meyer, T. J.; Conrad, D. *Inorg. Chem.* **1983**, *22*, 1617−1622.
(54) Caspar, J. V.; Meyer, T. J. *Inorg. Chem.* **1983**, *22*, 2444−2453.
(55) Rezvani, A. R.; Crutchley, R. J. *Inorg. Chem.* **1994**, *33*, 170−174.
(56) Li, Z.; Leed, N. A.; Dickson-Karn, N. M.; Dunbar, K. R.; Turro, C. *Chem. Sci.* **2013**, *5*, 727−737.
(57) Youngblood, W. J.; Lee, S. H.; Kobayashi, Y.; Hernandez-Pagan, E. A.; Hoertz, P. G.; Moore, T. A.; Moore, A. L.; Gust, D.; Mallouk, T. E. *J. Am. Chem. Soc.* **2009**, *131*, 926−927.
(58) Grätzel, M. *J. Photochem. Photobiol., C* **2003**, *4*, 145−153.
(59) Grätzel, M. *Acc. Chem. Res.* **2009**, *42*, 1788−1798.
(60) Nozik, A. J. *Appl. Phys. Lett.* **1976**, *29*, 150−153.
(61) Hanna, M. C.; Nozik, A. J. *J. Appl. Phys.* **2006**, *100*, 074510.